Discovery of Two Cyanobacterial Phenylalanine Ammonia Lyases: Kinetic and Structural Characterization[†,‡]

Michelle C. Moffitt,[§,||] Gordon V. Louie,[⊥] Marianne E. Bowman,[⊥] Janelle Pence,[||] Joseph P. Noel,*[,⊥] and Bradley S. Moore*[,§,||]

Scripps Institution of Oceanography and Skaggs School of Pharmacy and Pharmaceutical Sciences, University of California at San Diego, La Jolla, California 92093, College of Pharmacy, University of Arizona, Tucson, Arizona 85721, and Howard Hughes Medical Institute, Jack H. Skirball Center for Chemical Biology and Proteomics, The Salk Institute for Biological Studies, La Jolla, California 92037

Received August 28, 2006; Revised Manuscript Received November 20, 2006

ABSTRACT: Phenylalanine ammonia lyase (PAL) catalyzes the deamination of phenylalanine to cinnamate and ammonia. While PALs are common in terrestrial plants where they catalyze the first committed step in the formation of phenylpropanoids, only a few prokaryotic PALs have been identified to date. Here we describe for the first time PALs from cyanobacteria, in particular, *Anabaena variabilis* ATCC 29413 and *Nostoc punctiforme* ATCC 29133, identified by screening the genome sequences of these organisms for members of the aromatic amino acid ammonia lyase family. Both PAL genes associate with secondary metabolite biosynthetic gene clusters as observed for other eubacterial PAL genes. In comparison to eukaryotic homologues, the cyanobacterial PALs are 20% smaller in size but share similar substrate selectivity and kinetic activity toward L-phenylalanine over L-tyrosine. Structure elucidation by protein X-ray crystallography confirmed that the two cyanobacterial PALs are similar in tertiary and quatenary structure to plant and yeast PALs as well as the mechanistically related histidine ammonia lyases.

Phenylalanine ammonia lyases (PALs,[1] EC 4.3.1.5) catalyze the formation of *trans*-cinnamate via the nonoxidative deamination of L-Phe (*1*). PALs are ubiquitous in plants and catalyze the first committed step in the biosynthesis of several classes of plant phenylpropanoids. PALs are also commonly found in fungi. However, only a few examples of prokaryotic PALs are known, and these are associated with the biosynthesis of the secondary metabolites enterocin, cinnamide, and 3,5-dihydroxy-4-isopropylstilbene in the microorganisms *Streptomyces maritimus*, *Streptomyces verticillatus*, and *Photorhabdus luminescens*, respectively (*2*−*4*). PALs are members of a superfamily of ammonia lyases that also includes histidine ammonia lyase (HAL, EC 4.3.1.3) and tyrosine ammonia lyase (TAL). HALs, which are common in both eukaryotes and prokaryotes, share a common core three-dimensional structure with PALs and catalyze the deamination of L-His in the histidine degradation pathway (*1*). A few TALs that specifically deaminate L-Tyr to *p*-coumarate have been isolated to date; *p*-coumarate is used as a chromophore in the photoactive yellow protein of several species of purple phototropic bacteria, including *Rhodobacter capsulatus*, and is also utilized in the biosynthesis of the *Saccharothrix* natural product, saccharomicin (*5*, *6*). Recently, phenylalanine and tyrosine ammonia mutases were identified and found to be members of this extended superfamily. The aminomutases evolved specialized functions for the conversion of L-Phe and L-Tyr to the corresponding β-amino acids, the latter of which are then incorporated into the antitumor natural products paclitaxel and C-1027, respectively (*7*, *8*).

Crystal structures of HAL from the prokaryote *Pseudomonas putida* and PALs from parsley (*Petroselinum crispum*) and yeast (*Rhodosporidium toruloides*) have recently been reported (*9*−*11*). In total, these structure determinations showed that the ammonia lyases exist as homotetramers possessing a conserved polypeptide chain fold. The eukaryotic PALs are ∼20 kDa per monomer larger than the prokaryotic HALs, by virtue of a 54-residue N-terminal extension and an inserted 122-residue domain (*9*−*11*). The additional domain in the plant and fungal enzymes forms an arch over the active site and has been proposed to function as a shielding domain by restricting substrate entry and product egress (*10*). Alternatively, this domain may influence the conformation of an active-site lid loop and thereby affect the stability and catalytic activity of the holoenzyme (*12*, *13*). Crystallographic structures also established that the electrophilic prosthetic group required for catalytic activity

[†] This research was supported by the National Institutes of Health (Grant AI47808 to B.S.M.) and the National Science Foundation (Grant 0236027 to J.P.N.).

[‡] Atomic coordinates and structure factors have been deposited in the Protein Data Bank (entries 2NYN for *Av*PAL and 2NYF for *Np*PAL).

* To whom correspondence should be addressed. B.S.M.: telephone, (858) 822-6650; fax, (858) 558-3702; e-mail, bsmoore@ucsd.edu. J.P.N.: telephone, (858) 453-4100, ext. 1442; fax, (858) 597-0855; e-mail, noel@salk.edu.

[§] University of California.

[||] University of Arizona.

[⊥] The Salk Institute for Biological Studies.

[1] Abbreviations: PAL, phenylalanine ammonia lyase; *Av*PAL, *A. variabilis* phenylalanine ammonia lyase; *Np*PAL, *N. punctiforme* phenylalanine ammonia lyase; HAL, histidine ammonia lyase; MIO, 4-methylideneimidazole-5-one; PKU, phenylketonuria; rmsd, root-mean-square deviation; TAL, tyrosine ammonia lyase.

10.1021/bi061774g CCC: $37.00
Published on Web 01/05/2007

in this enzyme superfamily is 4-methylideneimidazole-5-one (MIO). MIO forms autocatalytically by cyclization and dehydration of a conserved active-site Ala-Ser-Gly tripeptide segment (*11*, *14*).

Medically significant is the fact that recombinant PAL is currently being evaluated for use in humans as enzyme substitution therapy for the treatment of the inherited metabolic disease phenylketonuria (PKU) (*13*, *15*, *16*). This disorder results from a mutation in the enzyme phenylalanine hydroxylase, thereby impairing the elimination of surplus L-Phe derived from the diet and causing severe neurotoxic effects. PAL is a viable candidate for enzyme inclusion as it efficiently reduces elevated L-Phe levels in the blood of PKU sufferers, converting excess L-Phe to the harmless metabolites cinnamic acid and ammonia. Animal models have demonstrated that the yeast *R. toruloides* PAL lowers blood L-Phe levels in PKU mice (*13*, *16*). Unfortunately, in vivo studies with the *R. toruloides* PAL identified problems associated with administration, immunogenicity, and stability of the enzyme.

In this study, we screened the prokaryotic genomes available in the NCBI database for putative PALs with the aim of identifying novel secondary metabolite biosynthetic pathways and new potential PKU therapeutic enzymes. Here, we report for the first time the identification of cyanobacterial PALs in the genomes of *Nostoc punctiforme* PCC73102 and *Anabaena variabilis* ATCC29413 and the biochemical characterization of these PALs in both wild-type and mutant forms. Protein X-ray crystallographic structure determination of the *A. variabilis* and *N. punctiforme* PALs reported here constitutes the first structural description of bacterial PALs and identifies the major structural differences between the eukaryotic and prokaryotic PALs.

MATERIALS AND METHODS

Construction of a Heterologous Expression Vector. The *A. variabilis* ATCC29413-U culture was obtained from the American Type Culture Collection (ATCC). The *N. punctiforme* ATCC29133 culture was provided by D. H. Sherman (University of Michigan, Ann Arbor, MI). Genomic DNA was isolated using a sodium dodecyl sulfate−lysozyme-based method as previously described (*17*). Genes encoding the putative PALs were amplified by PCR from *A. variabilis* genomic DNA using the primers AvppF.BamHI (5′-GGCGGATCCATGAAGACACTATCTCAAG-3′) and AvppR.NotI (5′-GTGCGGCCGCTTAATGCAAGCAGGGTAAG-3′) and *N. punctiforme* genomic DNA using the primers NppF.BamHI (5′-GGCGGATCCATGAATATAACATCTC-TAC-3′) and NppR.HindIII (5′-CGCAAGCTTTTACGT-TGACTTTAAGCTC-3′). The amplified genes were cloned using the Zero Blunt PCR cloning kit (Invitrogen) as described by the manufacturer. The inserts were excised from the resulting plasmids via BamHI and NotI or HindIII restriction digests. The gene fragment was separated from the vector DNA via agarose gel electrophoresis and purified from the agarose using the QIAquick gel extraction kit (Qiagen). Purified insert was then directionally ligated into the pHIS8 vector (*18*) such that the putative PAL protein would be expressed from the T7 promoter with an N-terminal octahistidyl tag and a thrombin cleavage site to remove the affinity tag. Alternatively, *N. punctiforme* genomic DNA was purchased from ATCC (29133D), and the PAL gene (ZP_00105927) was PCR-amplified with the oligonucleotides 5′-CACTGTCATATGAATATAACATCTCTA-CAACAGAACAT-3′ and 5′-GACAGTGGCGGCCGC-TCACGTTGACTTTAAGCTCGAAAAAATATG-3′. The resulting PCR product was digested with NdeI and NotI, and the 1.7 kb fragment was ligated into pET-28a(+) (Novagen).

Construction of Site-Directed Mutants. *Av*PAL mutants were generated using the QuikChange II site-directed mutagenesis kit (Stratagene, La Jolla, CA). L108A and L108G mutants were obtained using the L108A.F primer (5′-CAACTTAGTTTGGTTC**GCG**AAAACAGGTGCAGGG-3′) or the L108G.F primer (5′-CAACTTAGTTTGGTTC**G-GT**AAAACAGGTGCAGGG-3′), with the corresponding reverse complement oligonucleotide primer (mutations highlighted in bold). The *Av*PAL expression vector pMCM2571 DNA was used as a template. Mutations in the *Av*PAL gene were confirmed by sequencing.

Expression and Purification of His-Tagged PAL. For expression of either wild-type or mutant *Av*PAL, a single colony of *Escherichia coli* Rosetta 2(DE3) (Novagen), transformed with the pHIS8-*Av*PAL plasmid, was incubated in 4 mL of LB medium containing 50 mg/L kanamycin at 37 °C for 16 h. A flask containing 75 mL of TB medium with 50 mg/L kanamycin was inoculated with 2% (v/v) of the overnight seed culture. The expression culture was grown at 37 °C to an OD_{600} of approximately 1.0. Protein expression was induced via the addition of 0.05 mM IPTG, and cell growth was maintained at 22 °C for 16−18 h. The cells were then collected by centrifugation, frozen, and stored at −80 °C until they were needed.

For purification, thawed cells were resuspended in 12−15 mL of purification buffer [50 mM Tris-HCl (pH 8.0), 300 mM NaCl, 10% (v/v) glycerol, and 5 mM β-mercaptoethanol] containing 10 mM imidazole and lysed by sonication. The insoluble fraction was separated from soluble material via centrifugation at 15500*g* for 30 min. The soluble fraction was applied to a column containing 0.5 mL of Ni-NTA-agarose (Qiagen) and then washed three times with 5 mL of purification buffer containing 20 mM imidazole. The expressed protein containing the N-terminal octahistidyl tag was eluted from the column with 5 × 250 μL of purification buffer containing 250 mM imidazole. Purified protein was then exchanged into Tris-HCl storage buffer [100 mM Tris-HCl (pH 8.5), 2 mM EDTA, 2 mM DTT, and 10% (v/v) glycerol] using a PD-10 column (Pharmacia). The protein was either used immediately for enzyme assays or stored overnight at −80 °C prior to use. All protein samples were analyzed by denaturing PAGE using 7.5 or 10% SDS−polyacrylamide gels (Bio-Rad) and visualized using Bio-Safe Coomassie stain (Bio-Rad). The concentration of protein was determined using the Bio-Rad protein assay kit (Bio-Rad) compared to a bovine serum albumin standard curve or by measuring the absorbance at 280 nm from a calculated extinction coefficient for *Np*PAL of 0.807 g^{-1} L cm^{-1} at 280 nm and for *Av*PAL of 0.727 g^{-1} L cm^{-1} at 280 nm.

For crystallization studies, *Np*PAL was expressed using the plasmid pHIS8-*Np*PAL and purification was carried out essentially as described above for *Av*PAL, except for the use of an *E. coli* expression strain PlusE (www.exptec.com) that overexpresses the *E. coli* chaperone proteins GroEL and GroES. Alternatively, for kinetic studies, *Np*PAL was

expressed in *E. coli* BL21(DE3) cells (Stratagene) harboring pET-28-*Np*PAL and pGro7 (TaKaRa) and cultured in 25 mL of LB with 50 mg/L kanamycin and 20 mg/L chloramphenicol overnight at 37 °C. Twenty milliliters of this culture was seeded into 1 L of LB medium with kanamycin, chloramphenicol, and 0.5 mg/L L-arabinose and grown at 37 °C. At an OD_{600} of 0.6, the culture was chilled on ice. After 5 min, the culture was induced with 0.3 mM IPTG and grown for 16 h at 20 °C. Cells were harvested by centrifugation.

The harvested cells were resuspended in 100 mL of 50 mM Tris-HCl (pH 7.9) and 1 M NaCl and then passed two times through a pressure homogenizer (APV) operated at 12000−14000 psi. The homogenizer was washed with an additional 100 mL of buffer, and the wash was combined with the *E. coli* lysate. The combined mixture was placed in a water bath and heat-treated for 2 h at 55 °C, centrifuged at 10000*g*, and then filtered through a vacuum filter flask (0.2 μm, Nalgene).

The clarified lysate was passed over a column packed with 21 mL of Ni-NTA Superflow nickel resin (Qiagen), using an Akta Explorer 100 device (GE Healthcare). The column was washed with 3 column volumes of wash buffer [25 mM sodium phosphate (pH 7.0), 1 M NaCl, and 50 mM imidazole], and the His-tagged *Np*PAL eluted with a linear gradient over 10 column volumes of the wash buffer blended with elution buffer (wash buffer containing 0.5 M imidazole). Active fractions were pooled for further purification.

The active eluates were diluted 10-fold with 25 mM Tris-HCl (pH 7.8) and loaded onto a column packed with 7.7 mL of Macroprep High Q (Bio-Rad) resin. His-tagged *Np*PAL was eluted using a 10-column volume gradient from 0 to 0.5 M NaCl. Fractions were evaluated for purity by SDS−PAGE (Invitrogen) and pooled accordingly.

Phenylalanine Ammonia Lyase Activity Assays. For all kinetic studies, assays were performed in a final volume of 500 μL using 3.75 μg of *Av*PAL or 25 μg of *Np*PAL in 100 mM Tris-HCl (pH 8.5). Following preincubation of assay mixtures at 37 °C for 5 min, assays were initiated by the addition of L-Phe at final concentrations ranging from 10 to 200 μM. The assays were performed at 37 °C, and the formation of cinnamate was monitored continuously by UV spectroscopy at 280 nm ($\epsilon = 16\,890$ for *trans*-cinnamic acid) for 5 min (*19*).

To determine the optimal pH, assays were performed using 15 μg of protein, in 100 mM Tris-HCl at pHs ranging from 7.0 to 9.75 in a final volume of 500 μL. Following incubation at 37 °C for 5 min, assays were initiated by the addition of L-Phe to a final concentration of 200 μM. The assays were stopped after 15 min by adding 50 μL of concentrated HCl, and the absorbance was measured at 280 nm. Additionally, assays were performed as described above, at 30, 37, 40, and 45 °C to determine the optimal temperature. To determine activity with the substrates L-Tyr and L-His, the assay mixture contained 100 μg of protein and 100 mM Tris-HCl (pH 8.5) in a final volume of 1 mL. Assays were initiated by the addition of substrates to a final concentration of 200 μM. Formation of *p*-coumarate and urocanate was monitored for 16 h at 310 and 277 nm, respectively (*19*, *20*).

Crystallization of A. variabilis and N. punctiforme PALs. Crystals of *Av*PAL and *Np*PAL were grown from 1:1 mixtures of protein solution [~11 mg/mL in 12.5 mM Tris-HCl (pH 7.5) and 50 mM NaCl] and a reservoir solution. The crystallization mixtures (total volume of 2−3 μL) were equilibrated by hanging-drop vapor diffusion against reservoir solutions (500 μL) at 4 °C. The reservoir solutions contained 0.1 M MOPSO (pH 7.0), 7% (w/v) polyethylene glycol 8000, 0.2 M magnesium chloride, 10 mM cinnamic acid, and 2 mM dithiothreitol for *Av*PAL and 0.1 M MOPSO (pH 7.0), 21% (w/v) polyethylene glycol 8000, 0.2 M lithium sulfate, and 2 mM dithiothreitol for *Np*PAL. The *Av*PAL crystals grew as irregular blocks to a maximum size of 0.5 mm × 0.3 mm × 0.2 mm in the *P*1 space group with one homotetramer per unit cell per asymmetric unit. The *Np*PAL crystals grew as thin needle-shaped plates with maximum dimensions of 0.1 mm × 0.015 mm × 0.01 mm in the *I*222 space group with one molecule of *Np*PAL per asymmetric unit, in a tightly associated homotetramer generated by crystallographic symmetry.

X-ray Diffraction Data. For X-ray diffraction analyses, crystal samples were transferred to a cryoprotectant solution consisting of reservoir solution supplemented with 20% (v/v) glycerol and then mounted in nylon loops for freezing by immersion in liquid nitrogen. X-ray diffraction data were measured from frozen crystals, at beamline 8.2.2 of the Advanced Light Source (Lawrence Berkeley National Laboratory, Berkeley, CA) on an ADSC Quantum 315 CCD detector. Diffraction intensities were indexed, integrated, and scaled with XDS and XSCALE (*21*), or Denzo and Scalepack (*22*).

Determination of the X-ray Structures of A. variabilis and N. punctiforme PALs. The initial crystallographic structure solutions were obtained through molecular replacement analyses. Homology models were constructed with Modeler (*23*); the structure of parsley (*P. crispum*) PAL (PDB entry 1W27) served as a template for *Av*PAL, whereas a partially refined structure of *Av*PAL served as a template for *Np*PAL. Monomers of the PAL homology models were used for molecular replacement searches with Molrep (*24*). In the initial stages of the structure determination of *Av*PAL, the protein model was rebuilt extensively against an electron density map improved by 4-fold, noncrystallographic symmetry (NCS) averaging. Xfit (*25*) was used for map inspection and manipulation of the atomic model. CNS was used for structural refinement used (*26*). For *Av*PAL, NCS restraints were applied until the final stages of refinement. Programs from the CCP4 (*27*) suite were employed for all other crystallographic calculations.

RESULTS

Discovery of Two Cyanobacterial Phenylalanine Ammonia Lyases. The putative PALs from *A. variabilis* ATCC 29413 (Ava_3988, *Av*PAL, 567 residues) and *N. punctiforme* ATCC 29133 (Npun02008223, *Np*PAL, 569 residues) were identified by searching completed cyanobacterial genomes for homologues of the *S. maritimus* PAL, EncP (*4*). This approach identified at least two putative cyanobacterial PAL enzymes that were each annotated initially as HALs. The *A. variabilis* and *N. punctiforme* proteins were predicted to have PAL activity as they contained an aliphatic residue conserved in the active site of known PAL enzymes thought to be associated with substrate specificity (Supporting Information) (*28*). These two cyanobacterial PALs are 77% identical in

Table 1: Kinetic Analysis of *Av*PAL and *Np*PAL Wild-Type Enzymes and Comparison with *Av*PAL Mutants

	K_m (mM)	k_{cat} (s^{-1})	k_{cat}/K_m (mM^{-1} s^{-1})
*Av*PAL[a]	0.060 ± 0.005	4.3 ± 0.4	72.2
*Np*PAL[a]	0.045	1.96	43.8
L108A[a]	0.069 ± 0.006	3.6 ± 0.3	52.5
L108G[a]	0.07 ± 0.02	0.95 ± 0.02	14.6
*Av*PALΔ21[a]	0.06 ± 0.01	4.6 ± 0.8	73.7
Ps. putida PAL (*34*)	0.12 ± 0.004	13.5 ± 0.1	112.5
S. maritimus PAL (*29*)	0.023 ± 0.005	$4.70 \times 10^{-3} \pm 0.28 \times 10^{-3}$	0.208

[a] From this study. Kinetic analysis was performed at 37 °C and pH 8.5.

amino acid sequence and are significantly similar in sequence to plant PAL enzymes, although they are more similar in size (*Av*PAL has 567 residues and *Np*PAL 569 residues) to the smaller prokaryotic HAL enzymes (*Ps. putida* HAL has 509 residues) than the larger plant PAL enzymes (*P. crispum* PAL has 715 residues). Consistent with the association of bacterial PALs with secondary metabolite biosynthetic clusters, the *Av*PAL gene was identified upstream of genes encoding a mixed nonribosomal peptide synthetase and polyketide synthase pathway, while the *Np*PAL gene appeared to be associated with an unusual fatty acid biosynthetic gene cluster (data not shown).

Expression and Characterization of Recombinant Anabaena and Nostoc PAL. Gene fragments encoding the putative *A. variabilis* and *N. punctiforme* PALs were amplified by PCR from genomic DNA of these organisms and ligated into *E. coli* expression vectors. *Av*PAL was readily expressed as soluble His-tagged protein in *E. coli*. However, initial attempts to express the *Np*PAL in *E. coli* yielded predominantly insoluble protein, and the production of significant levels of soluble His-tagged *Np*PAL protein in *E. coli* required the coexpression of GroES and GroEL chaperone proteins to facilitate correct folding of the PAL protein in the host. Following Ni-NTA affinity purification of the His-tagged proteins, both cyanobacterial PALs were confirmed to be 64 kDa in size by PAGE.

Preliminary in vitro studies confirmed that both enzymes possessed PAL activity converting L-phenylalanine to cinnamate as determined by HPLC−MS analysis with an authentic standard as a control (data not shown). Further characterization showed that *Av*PAL had no detectable activity with L-His, although the formation of *p*-coumarate from L-Tyr could be detected after prolonged incubation. The activity of *Av*PAL in Tris-HCl was found to be optimal at pH 8.5 (Supporting Information) and 40 °C.

Kinetic Analyses of the Cyanobacterial PALs. To compare the activity of the two cyanobacterial PALs, kinetic studies of *Av*PAL and *Np*PAL were conducted. In both cases, kinetic constants were estimated from linear Hanes plots. The cyanobacterial PALs were analyzed at 37 °C and pH 8.5 and were shown to have comparable enzymatic activity (Table 1). The k_{cat} values of wild-type *Av*PAL and *Np*PAL were determined to be approximately 500−1000-fold greater than that of the previously characterized bacterial PAL, EncP from *S. maritimus* (k_{cat} = 0.0048 s^{-1} and k_{cat}/K_m = 0.21 mM^{-1} s^{-1} at 30 °C and pH 8.8) (*29*) but approximately 3-fold lower than that of *P. crispum* PAL (k_{cat} = 13.5 s^{-1} and k_{cat}/K_m = 112.5 mM^{-1} s^{-1} at 30 °C and pH 8.8) (*28*).

Table 2: Statistics for X-ray Diffraction Data and Structural Refinement of *Av*PAL and *Np*PAL

	*Av*PAL	*Np*PAL
crystal form		
space group	*P*1	*I*222
unit cell parameters	a = 78.2 Å, b = 88.5 Å, c = 90.1 Å; α = 103.5°, β = 97.8°, γ = 116.2°	a = 74.3 Å, b = 91.5 Å, c = 151.1 Å
no. of monomers per asymmetric unit	4	1
X-ray diffraction data		
resolution range (Å)	100−1.90	100−2.50
no. of reflections measured	325535	81381
merging *R*-factor	0.073 (0.289)	0.098 (0.475)
mean $I/\sigma I$	7.94 (3.20)	12.56 (1.75)
completeness	0. 948 (0.884)	0. 929 (0.697)
redundancy	2.15 (2.10)	4.80 (2.80)
structure refinement		
no. of reflections used	151571	15884
R-factor	0.230 (0.299)	0.247 (0.320)
R_{free}	0.247 (0.341)	0.305 (0.357)
no. of amino acid residues	2056	513
no. of water molecules	537	31
residues with most favorable conformation (%)	92.2	92.4

A. variabilis Mutagenesis and Analysis. In previous studies of ammonia lyases, a number of active-site residues were proposed to be responsible for conferring substrate selectivity for L-His or L-Phe (*1, 28*). One residue of interest, His 83 (*Ps. putida* numbering), in HAL is thought to orient L-His in the active site, whereas the substitution of more hydrophobic residues at the corresponding position in PAL proteins may serve to better accommodate the substrate L-Phe (*28*). Recently, in an effort to determine the function of Val 83 in the *S. maritimus* PAL EncP, V83H and V83A mutants were generated and characterized (*29*). Curiously, while the EncP V83H mutant lost all lyase activity, the EncP V83A mutant was more active than the wild-type enzyme with the substrate L-Phe. In this study, Ala and Gly substitutions of *Av*PAL were introduced at the corresponding aliphatic residue, Leu 108. Expression of both mutants in *E. coli* generated soluble His-tagged protein. There was a slight decrease in PAL activity of the L108A mutant as compared to the wild-type enzyme (Table 1). Kinetic activity was further decreased in the L108G mutant (Table 1).

On the basis of sequence alignments, both *Av*PAL and *Np*PAL contain an additional 21-amino acid N-terminal extension that is absent from *S. maritimus* EncP PAL and related HALs. In an effort to ascertain the role of the N-terminal extension on *Av*PAL activity, we generated a truncated mutant by removing the first 21 amino acids. Heterologous expression of the truncated *Av*PAL in *E. coli* yielded soluble active protein. The kinetic parameters of the truncated mutant did not differ significantly from those of the wild-type enzyme (Table 1). This indicates that the removal of the 21-amino acid N-terminal region had no adverse effects on the in vitro catalytic activity of *Av*PAL.

Crystal Structure of A. variabilis and N. punctiforme Phenylalanine Ammonia Lyases. As expected from the high degree of sequence identity (~75% with no insertions or deletions) between *Av*PAL and *Np*PAL, the tertiary and quaternary structures of the two proteins (Figure 1c of the Supporting Information) are highly similar. The PALs exist as homotetramers with 222-point symmetry (Figure 1A). Within a homotetramer, each of the four identical active sites

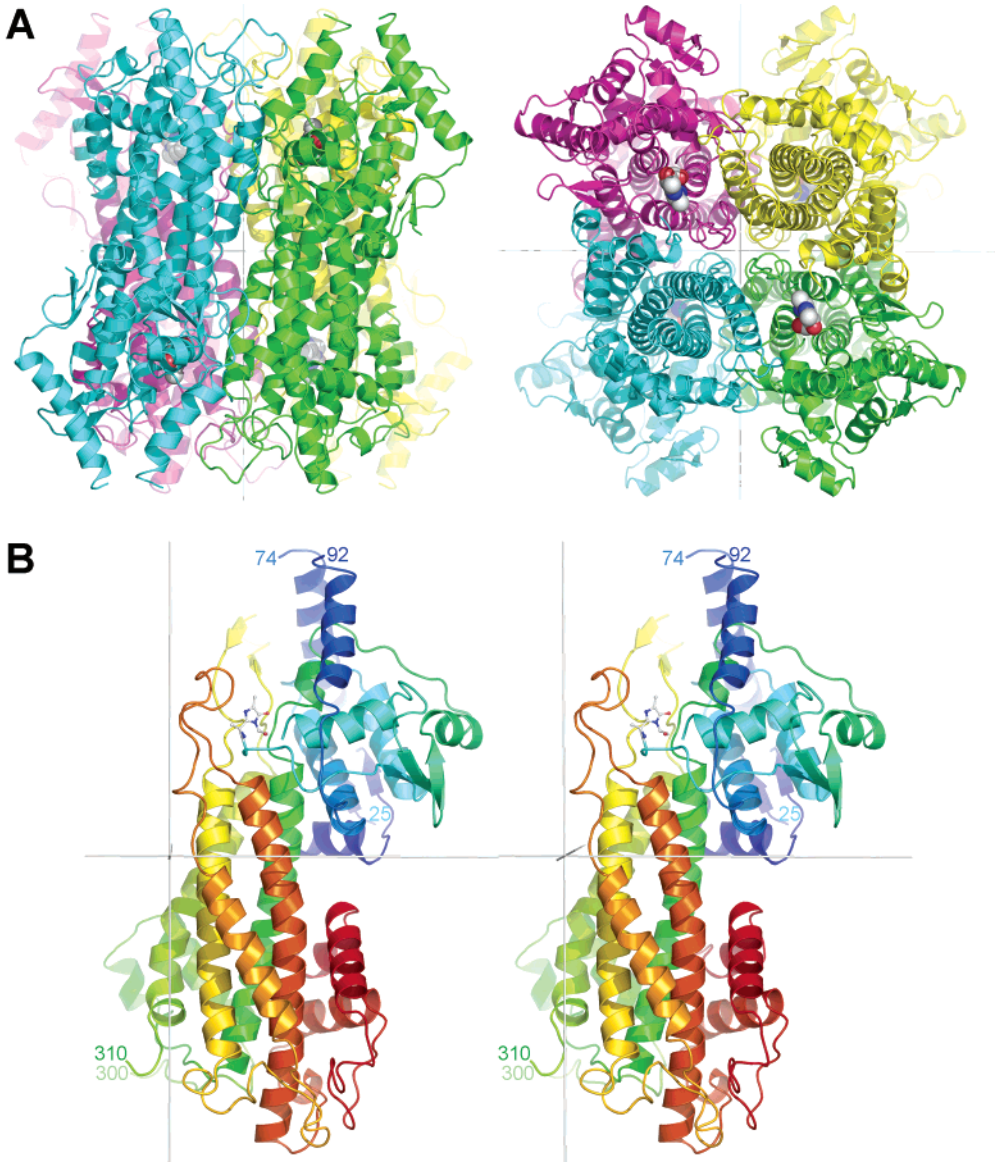

FIGURE 1: Structure of cyanobacterial PAL homotetramers and monomers. (A) Ribbon representation of the *Av*PAL homotetramer, with the polypeptide chains of four individual monomers: A (green), B (cyan), C (magenta), and D (yellow). The atoms of the four MIO prosthetic groups are drawn as spheres. The left panel shows a view from the side of the core helical bundles of the four monomers; the right panel shows a top view, into the active-site clefts of two of the monomers. The 222-point symmetry of the homotetramer is generated by three mutually orthogonal and intersecting 2-fold axes (gray lines; two of the axes are visible in each orientation, with the third perpendicular to these two). (B) Stereo ribbon representation of a monomer of *Av*PAL. The polypeptide chain is colored according to the colors of the rainbow, with blue for the N-terminus and red for the C-terminus. Two poorly ordered loops (residues 75−91 and 301−309) are not included in the structure. The atoms of MIO, formed by residues Ala 167, Ser 168, and Gly 169 of this polypeptide chain, are drawn as balls and sticks. The 2-fold axes that relate this monomer to the other monomers in the homotetramer are shown as gray lines. This orientation corresponds to a left-side view of the green monomer in panel A. This orientation is maintained roughly in all subsequent figures, except for Figure 2.

is formed by three distinct monomeric subunits. The polypeptide chain fold of a PAL monomer is predominantly α-helical (Figure 1A,B), with a central, up−down bundle of five α-helices. These helices, together with a long hairpin loop joining the last two helices of the bundle, form the intersubunit interfaces at the core of the homotetramer. Two subdomains form at the ends of the central bundle. The N-terminal segment of the polypeptide chain constitutes the bulk of a subdomain that carries the MIO prosthetic group. The C-terminal segment forms a peripheral layer of α-helices, which wraps around the end of the central bundle. This subdomain contributes additional intersubunit contacts that stabilize the homotetramer, and most importantly, it projects a key loop into the active-site cavity of an adjacent monomer.

The cyanobacterial PALs are very similar structurally to the PALs from parsley (*P. crispum*; PDB entry 1W27) and yeast (*R. toruloides*; PDB entries 1T6P and 1Y2M) and *Ps. putida* HAL (PDB entry 1GKM). From a comparison of the superposed polypeptide chain backbones of the ammonia lyase structures, *Av*PAL differs from parsley PAL by a 1.4 Å rmsd for 448 equivalent residues (with 36% identical sequence), from yeast PAL by a 1.1 Å rmsd for 463 equivalent residues (34% identical sequence), and from *Ps. putida* HAL by a 1.5 Å rmsd for 450 equivalent residues (29% identical sequence). Interestingly, although the cyanobacterial PALs are more similar in size to the bacterial HAL (all of the bacterial ammonia lyases lack two polypeptide segments present in the eukaryotic PALs, a long N-terminal

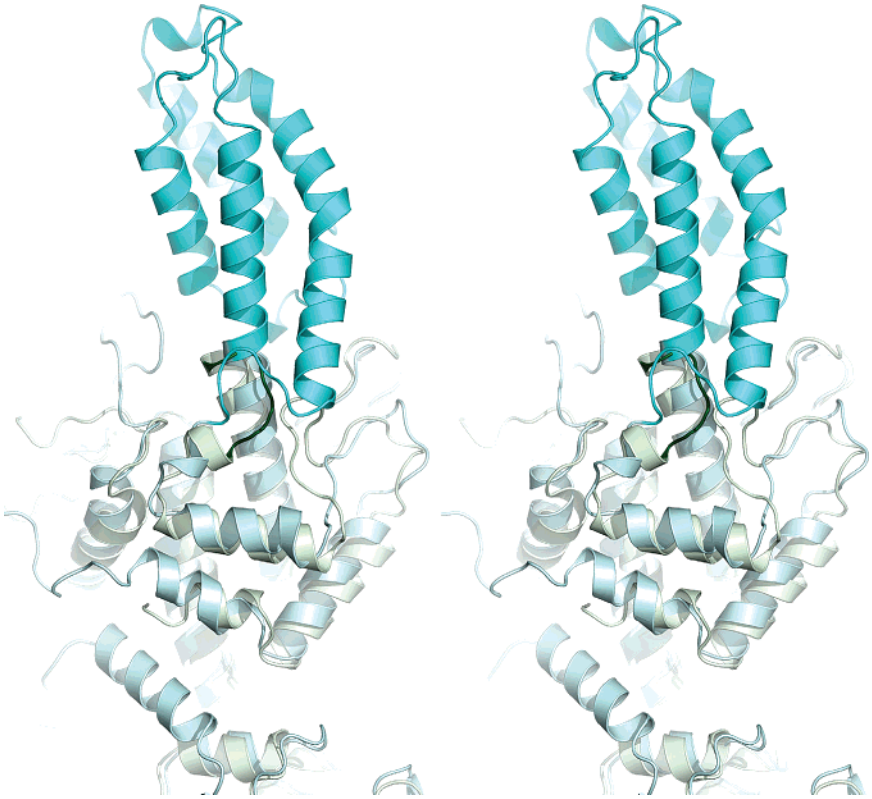

FIGURE 2: Comparison of the polypeptide chain backbones of monomers of *Av*PAL (green) and parsley PAL (cyan). Only regions in the vicinity of the inserted shielding domain of parsley PAL (highlighted in darker cyan) are shown. In *Av*PAL, the shielding domain is replaced with a short loop (dark green).

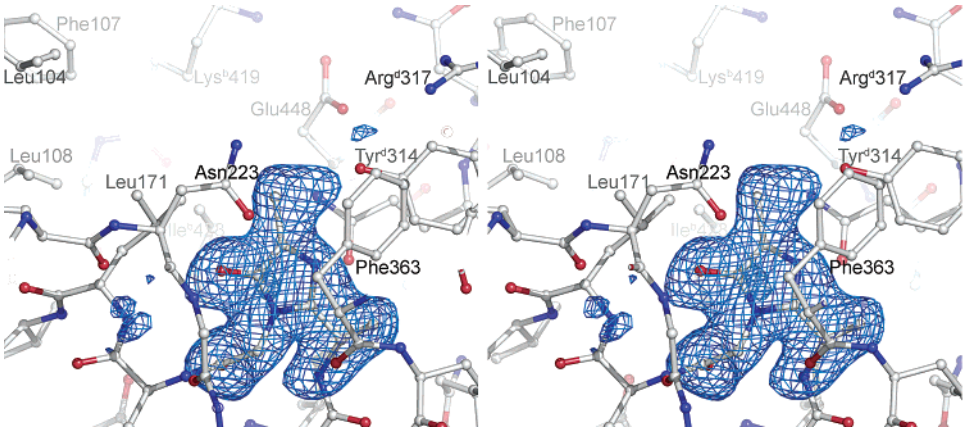

FIGURE 3: Stereoview of the methylideneimidazolone prosthetic group and protein residues forming the active-site pocket. Protein atoms are drawn as balls and sticks and are colored by element (gray for carbon, blue for nitrogen, and red for oxygen). Hydrogen bonding interactions formed by MIO are represented as green dashed lines. An oxyanion hole is formed by the backbone amide nitrogens of Leu 172 and Gly 225. The blue-colored contours envelop regions greater than 3σ in the MIO omit electron density map (coefficients [$F_o - F_c'$]ϕ_c', where F_c' and ϕ_c' were calculated without a contribution from atoms of the MIO).

extension, and an additional domain near the C-terminus), the cyanobacterial PALs are more similar structurally to yeast and parsley PAL. The additional domain, termed the shielding domain (*10*), represents an insertion in the polypeptide chain of the eukaryotic PALs immediately after the helical bundle. In these PALs, the first α-helix of the shielding domain extends helix 5 of the core bundle, whereas in the cyanobacterial PALs, the much shorter helix 5 is followed by a small connecting segment that leads immediately into the peripheral α-helices of the C-terminal domain (Figure 2).

MIO and Modeling of Substrate in the Active Site. The active-site cleft of the ammonia lyases is located above the exocyclic methylidene carbon of the MIO prosthetic group. The MIO of the cyanobacterial PALs, formed by residues Ala 167, Ser 168, and Gly 169, is clearly defined in electron density maps (Figure 3). The imidazolone ring is stacked against the side chain of Phe 363, with an interplanar separation of ~4 Å. The MIO N168 atom accepts a hydrogen bond from the Tyr^{D} 314 OH group. [In this and subsequent descriptions, residue numbering refers to the polypeptide chain of a single monomer (A); residues designated with a superscripted B, C, or D are contributed by a dyad-related monomer of the homotetramer.] The other MIO atom available for polar interactions, O168, forms a hydrogen bond with the side chain of Asn 223 and is also directed into a

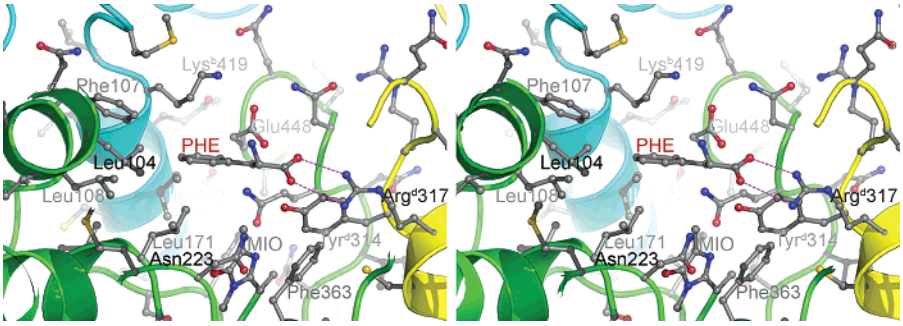

FIGURE 4: Modeled binding of the L-Phe substrate to *Av*PAL. Hydrogen bonding interactions formed between the carboxylate group of the L-Phe substrate and the δ-guanidino group of Arg 317 of *Av*PAL are represented as magenta dashed lines. Polypeptide chain backbones of *Av*PAL are represented as ribbons and colored according to monomer as in Figure 3.

small pocket lined by the backbone amide nitrogens of Leu 171 and Gly 224.

Although no direct structural information about the binding of the L-Phe substrate within the active site of the PALs is available, recently described crystallographic analyses of TAL from *R. capsulatus* (*30*) now support reliable predictive modeling. These analyses have identified in TAL an active-site His that plays a pivotal role in conferring selectivity for L-Tyr. This His occurs adjacent to *Ps. putida* HAL position 83, which was identified as a potential specificity determinant in earlier studies (see above). Replacement of this His with Phe effectively converts the TAL into a phenylalanine-specific ammonia lyase, and the crystal structure of this mutant TAL in complex with the reaction product cinnamic acid provides a basis for the structural modeling of binding of L-Phe to native PAL enzymes. The key interactions made by the L-Phe molecule in the modeled complex with *Av*PAL (Figure 4) are a salt bridge between the substrate's α-carboxylate and the δ-guanidino group of Arg 317 and an aromatic, edge−edge interaction between the substrate's phenyl ring and the side chain of Phe 107. Notably, Phe 107 replaces the key, substrate-specificity-determining His in TAL. Proposed chemical mechanisms of the ammonia lyase family of enzymes, based on cocrystallization of the product with TAL, are discussed by Louie et al. (*30*).

In the cyanobacterial PAL structures, two disordered polypeptide chain segments (residues 75−91 and 301−309) are located near the entrance to the active-site cleft. In TAL, the first of these segments is packed tightly within the active-site cleft and interacts closely with the bound substrate and/or product molecule, whereas the second segment forms a more external loop that caps the active-site region. These loops appear to be intrinsically flexible in the PAL proteins, as they are also poorly ordered in the structures of parsley and yeast PAL (*9*, *10*). In the crystal structures of the cyanobacterial PALs, the active-site cleft appears to be very exposed to the external solvent, and the absence of stabilizing interactions contributed by the disordered inner loop is a likely reason for the failure to observe stable binding to these PALs of the substrate (L-Phe), the product (cinnamic acid), and a potent PAL-specific inhibitor (2-aminoindan-2-phosphonic acid) (*31*).

DISCUSSION

In this study, we report the discovery and characterization of phenylalanine ammonia lyases (PAL) in the cyanobacteria *A. variabilis* and *N. punctiforme*. Although histidine ammonia lyases (HALs) are common in prokaryotes, PALs have been identified in the genomes of only a few prokaryotes to date. In vitro characterization confirmed that both *Av*PAL and *Np*PAL share many characteristics with eukaryotic PALs, including an optimal pH of 8.5 and some relaxed selectivity possessing the ability to turn over L-Tyr. The catalytic activities of the cyanobacterial PALs were similar to those of other plant PALs and significantly better than those of the previously characterized *Streptomyces* PAL, EncP (*29*), and *Photobacteria* PAL, StlA (*3*). On the basis of analysis of the ORFs flanking the PAL genes, we predict that the cyanobacterial PALs generate a cinnamic acid product that is utilized in the biosynthesis of a specialized metabolite. To the best of our knowledge, the end products of these pathways have not been identified in *A. variabilis* and *N. punctiforme* to date.

Elucidation of the crystal structures of *A. variabilis* and *N. punctiforme* PAL established that the cyanobacterial PALs share the same overall structural fold as previously characterized members of the aromatic amino acid ammonia lyase family. The eukaryotic PALs are distinguished structurally from the prokaryotic ammonia lyases by their larger size, which results primarily from the 54-residue N-terminal extension, the inserted shielding domain, and some other small inserted segments (*10*). On the basis of structural and sequence homology, the prokaryotic PALs and TALs are proposed to have evolved from bacterial HAL. Similarly, eukaryotic PAL probably evolved from bacterial HAL, although this is likely to have occurred much earlier in time (*10*). It is therefore interesting to note that the cyanobacterial PALs, while similar in size to the bacterial HALs, are structurally more similar to the eukaryotic PALs. Thus, we propose that the cyanobacterial PALs may represent an evolutionary intermediate from which the eukaryotic PALs were derived. While a number of roles for the eukaryotic specific subdomains have been proposed, studies to date of these bacterial PAL/TALs have thus far failed to elucidate a clear role for these eukaryote-specific evolutionary additions.

*Av*PAL and *Np*PAL both contain an N-terminal extension of approximately 20 residues, relative to *Ps. putida* HAL and *S. maritimus* EncP PAL, which is disordered in the crystal structures. The beginning of the ordered region of the polypeptide chain (Asn 25 in *Av*PAL and Val 26 in *Np*PAL) resides near the initial residue of the first β-strand. The N-terminal extensions of these cyanobacterial PALs therefore differ structurally from the even longer N-terminal

segment in parsley PAL, which is ordered and forms a helical segment that packs against the equivalent segment from another monomer within the homotetramer. Biochemical characterization of the truncated *Av*PAL with an N-terminal deletion of 21 residues showed that enzyme activity was not significantly different from that of the full-length protein. Therefore, the N-terminal segment is unlikely to play a role in catalysis, consistent with its positioning on the surface of the homotetramer remote from the active site. Whereas the full-length *Av*PAL formed crystals readily, crystallization attempts under similar conditions with the *Av*PAL truncated mutant were less successful and instead yielded large amounts of aggregated protein. This observation is perhaps indicative of the altered surface properties and solubility of the truncated *Av*PAL protein.

Mutants were generated within the predicted substrate binding pocket of *Av*PAL based upon previously reported studies of wild-type and V83-replaced *Streptomyces* PAL, EncP (*29*). While the *Streptomyces* V83A mutant enzyme exhibited improved catalytic activity, the corresponding Ala replacement (L108A) and also a Gly replacement (L108G) in the *Av*PAL enzyme resulted in decreased catalytic activity. Comparison of PAL amino acid sequences shows the residues that form the predicted binding pocket for the L-Phe substrate's benzene ring are in general highly conserved. As expected, this binding pocket is predominantly hydrophobic in character and is formed by the side chains of Leu 104, Phe 107, Leu 108, and Leu 171 (*Av*PAL numbering). In *Av*PAL, the slight decreases in enzyme activity caused by Ala and Gly replacements of Leu 108 are consistent with the loss of favorable nonpolar contacts to the substrate's phenyl ring. EncP PAL from *S. maritimus* (*29*) is unusual, as there are significant differences in the identity of the residues that constitute the L-Phe binding pocket (Figure 4 of the Supporting Information). For example, a Phe residue (at position 403, which replaces Ile 423 in *Av*PAL) from an adjacent monomer protrudes prominently into the substrate-binding pocket and likely provides the primary interaction surface for the phenyl ring of the L-Phe substrate. As a result, two smaller residues, Ala 82 and Val 83, replace the characteristic Phe-Leu sequence. Therefore, for EncP, the altered positioning of nonpolar side chains within the substrate-binding pocket may explain the atypical behavior of mutant proteins with amino acid replacements of Val 83. An Ala substitution further enlarges the binding pocket while maintaining the pocket's nonpolar character and results in an enhancement in enzyme activity. In contrast, replacement of Val 83 with the larger and more polar His side chain abolishes activity.

In the future, PALs may have applications in enzyme substitution therapy for reducing toxic levels of L-Phe in the blood of PKU patients by converting it to the harmless products cinnamate and ammonia (*13*, *15*, *16*, *32*, *33*). While both the yeast and parsley PALs have been extensively evaluated as a potential therapeutic enzyme through in vivo studies, several factors have impeded their development into the clinic (*13*, *15*, *16*, *32*, *33*). These include development of an immune response over time when administered parenterally and sensitivity to proteases when administered enterally (*15*). The most accessible chymotrypsin and trypsin cleavage sites within the yeast PAL are located in a flexible active-site loop (*13*, *15*). While protease-protected variants of yeast PAL have been engineered, the mutant enzymes have significantly lower specific activity and a large dose of the engineered PAL is necessary to affect lowered plasma L-Phe levels. The newly discovered cyanobacterial PALs represent alternatives to the yeast PAL for future in vivo studies.

Both cyanobacterial PALs have catalytic activity comparable to that of the plant and yeast enzymes and have the advantage of being significantly smaller. The smaller cyanobacterial PALs lack the protease-sensitive lid loop (*13*) found in all eukaryotic PALs and are predicted to be less sensitive to proteases and thus have greater in vivo stability. Other sites targeted by human proteases can be identified in the cyanobacterial PALs and engineered accordingly. We have shown in this study that the 21-amino acid extension at the N-terminus, which contains chymotrypsin/trypsin target amino acids Lys, Phe, and Trp, can be removed from *Av*PAL with no adverse effects on activity in vitro. To prevent an immune response to PAL in vivo, recent studies have shown that yeast and parsley PAL can be derivatized with PEG at surface-exposed Lys residues. The chemically modified enzyme retains all catalytic activity, has an extended catalytic half-life, and has a reduced immunogenicity when administered subcutaneously (*13*, *32*, *33*). Similar studies could be performed with the cyanobacterial PALs. Analyses of the crystal structures show that both cyanobacterial enzymes possess 11 surface-exposed Lys residues, and another three Lys residues in disordered regions are also likely to be surface-exposed (Supporting Information). Using these data, the pattern of PEG derivitization can be predicted. Where necessary, additional PEG attachment sites can be created by strategically engineering new surface-exposed Lys residues. The biochemical and structural characterization of cyanobacterial PALs reported in this paper, together with further structure-based chemical modification studies, could be used to engineer new PKU therapeutic enzymes with beneficial structural, biochemical, and/or immunogenic properties.

ACKNOWLEDGMENT

We are grateful to Michael Vellard, Joshua Bliesath, and Yanhong Zhang (BioMarin Pharmaceutical) for establishing the kinetic results for *Np*PAL and for useful discussions.

SUPPORTING INFORMATION AVAILABLE

A figure comparing residues in the active site of plant PAL, bacterial HAL, and cyanobacterial homologues used to predict substrate specificity in HALs and PALs, a graph showing the activity of *A. variabilis* PAL at various pHs, a figure showing the molecular surface of the *Av*PAL homotetramer and the location of surface-exposed Lys residues, a figure representing the superposition of the polypeptide chain backbones of monomers of *Av*PAL and *Np*PAL, a figure comparing the substrate-binding pockets of *Av*PAL and modeled *S. maritimus* PAL (EncP). This material is available free of charge via the Internet at http://pubs.acs.org.

REFERENCES

1. Poppe, L., and Rétey, J. (2005) Friedel-Crafts-type mechanism for the enzymatic elimination of ammonia from histidine and phenylalanine, *Angew. Chem., Int. Ed. 44*, 3668−3688.

2. Bezanson, G. S., Desaty, D., Emes, A. V., and Vining, L. C. (1970) Biosynthesis of cinnamamide and detection of phenylalanine ammonia-lyase in *Streptomyces verticillatus*, *Can. J. Microbiol. 16*, 147−151.
3. Williams, J. S., Thomas, M., and Clarke, D. J. (2005) The gene *stlA* encodes a phenylalanine ammonia-lyase that is involved in the production of a stilbene antibiotic in *Photorhabdus luminescens* TT01, *Microbiology 151*, 2543−2550.
4. Xiang, L., and Moore, B. S. (2002) Inactivation, complementation, and heterologous expression of *encP*, a novel bacterial phenylalanine ammonia-lyase gene, *J. Biol. Chem. 277*, 32505−32509.
5. Berner, M., Krug, D., Bihlmaier, C., Vente, A., Muller, R., and Bechthold, A. (2006) Genes and enzymes involved in caffeic acid biosynthesis in the actinomycete *Saccharothrix espanaensis*, *J. Bacteriol. 188*, 2666−2673.
6. Kyndt, J. A., Meyer, T. E., Cusanovich, M. A., and Van Beeumen, J. J. (2002) Characterization of a bacterial tyrosine ammonia lyase, a biosynthetic enzyme for the photoactive yellow protein, *FEBS Lett. 512*, 240−244.
7. Christenson, S. D., Liu, W., Toney, M. D., and Shen, B. (2003) A novel 4-methylideneimidazole-5-one-containing tyrosine aminomutase in enediyne antitumor antibiotic C-1027 biosynthesis, *J. Am. Chem. Soc. 125*, 6062−6063.
8. Walker, K. D., Klettke, K., Akiyama, T., and Croteau, R. (2004) Cloning, heterologous expression, and characterization of a phenylalanine aminomutase involved in Taxol biosynthesis, *J. Biol. Chem. 279*, 53947−53954.
9. Calabrese, J. C., Jordan, D. B., Boodhoo, A., Sariaslani, S., and Vannelli, T. (2004) Crystal structure of phenylalanine ammonia lyase: Multiple helix dipoles implicated in catalysis, *Biochemistry 43*, 11403−11416.
10. Ritter, H., and Schulz, G. E. (2004) Structural basis for the entrance into the phenylpropanoid metabolism catalyzed by phenylalanine ammonia-lyase, *Plant Cell 16*, 3426−3436.
11. Schwede, T. F., Rétey, J., and Schulz, G. E. (1999) Crystal structure of histidine ammonia-lyase revealing a novel polypeptide modification as the catalytic electrophile, *Biochemistry 38*, 5355−5361.
12. Pilbak, S., Tomin, A., Rétey, J., and Poppe, L. (2006) The essential tyrosine-containing loop conformation and the role of the C-terminal multi-helix region in eukaryotic phenylalanine ammonia-lyases, *FEBS Lett. 273*, 1004−1019.
13. Wang, L., Gamez, A., Sarkissian, C. N., Straub, M., Patch, M. G., Han, G. W., Striepeke, S., Fitzpatrick, P., Scriver, C. R., and Stevens, R. C. (2005) Structure-based chemical modification strategy for enzyme replacement treatment of phenylketonuria, *Mol. Genet. Metab. 86*, 134−140.
14. Baedeker, M., and Schulz, G. E. (2002) Autocatalytic peptide cyclization during chain folding of histidine ammonia-lyase, *Structure 10*, 61−67.
15. Sarkissian, C. N., and Gamez, A. (2005) Phenylalanine ammonia lyase, enzyme substitution therapy for phenylketonuria, where are we now? *Mol. Genet. Metab. 86* (Suppl. 1), S22−S26.
16. Sarkissian, C. N., Shao, Z., Blain, F., Peevers, R., Su, H., Heft, R., Chang, T. M., and Scriver, C. R. (1999) A different approach to treatment of phenylketonuria: Phenylalanine degradation with recombinant phenylalanine ammonia lyase, *Proc. Natl. Acad. Sci. U.S.A. 96*, 2339−2344.
17. Neilan, B. A., Jacobs, D., and Goodman, A. E. (1995) Genetic diversity and phylogeny of toxic cyanobacteria determined by DNA polymorphisms within the phycocyanin locus, *Appl. Environ. Microbiol. 61*, 3875−3883.
18. Jez, J. M., Ferrer, J. L., Bowman, M. E., Dixon, R. A., and Noel, J. P. (2000) Dissection of malonyl-coenzyme A decarboxylation from polyketide formation in the reaction mechanism of a plant polyketide synthase, *Biochemistry 39*, 890−902.
19. Kalghatgi, K. K., and Subba, Rao, P. V. (1975) Microbial L-phenylalanine ammonia-lyase. Purification, subunit structure and kinetic properties of the enzyme from *Rhizoctonia solani*, *Biochem. J. 149*, 65−72.
20. Tabor, H., and Mehler, A. H. (1955) Histidase and urocanase, *Methods Enzymol. 2*, 228−233.
21. Kabsch, W. (1993) Automatic processing of rotation diffraction data from crystals of initially unknown symmetry and cell constants, *J. Appl. Crystallogr. 26*, 795−800.
22. Otwinowski, Z., and Minor, W. (1997) Processing of X-ray diffraction data collected in oscillation mode, *Methods Enzymol 276*, 307−326.
23. Sali, A., and Blundell, T. L. (1993) Comparative protein modelling by satisfaction of spatial restraints, *J. Mol. Biol. 234*, 779−815.
24. Vagin, A., and Teplyakov, A. (1997) MOLREP: An automated program for molecular replacement, *J. Appl. Crystallogr. 30*, 1022−1025.
25. McRee, D. E. (1999) XtalView/Xfit: A versatile program for manipulating atomic coordinates and electron density, *J. Struct. Biol. 125*, 156−165.
26. Brunger, A. T., Adams, P. D., Clore, G. M., DeLano, W. L., Gros, P., Grosse-Kunstleve, R. W., Jiang, J. S., Kuszewski, J., Nilges, M., Pannu, N. S., Read, R. J., Rice, L. M., Simonson, T., and Warren, G. L. (1998) Crystallography & NMR system: A new software suite for macromolecular structure determination, *Acta Crystallogr. D54*, 905−921.
27. Collaborative Computational Project Number 4 (1994) The CCP4 suite: Programs for protein crystallography, *Acta Crystallogr. D50*, 760−763.
28. Rother, D., Poppe, L., Morlock, G., Viergutz, S., and Rétey, J. (2002) An active site homology model of phenylalanine ammonia-lyase from *Petroselinum crispum*, *Eur. J. Biochem. 269*, 3065−3075.
29. Xiang, L., and Moore, B. S. (2005) Biochemical characterization of a prokaryotic phenylalanine ammonia lyase, *J. Bacteriol. 187*, 4286−4289.
30. Louie, G. V., Bowman, M. E., Moffitt, M. C., Baiga, T. J., Moore, B. S., and Noel, J. P. (2006) Structural determinants and modulation of substrate specificity in phenylalanine−tyrosine ammonia lyases, *Chem. Biol. 13*, 1327−1338.
31. Appert, C., Zon, J., and Amrhein, N. (2003) Kinetic analysis of the inhibition of phenylalanine ammonia-lyase by 2-aminoindan-2-phosphonic acid and other phenylalanine analogues, *Phytochemistry 62*, 415−422.
32. Gamez, A., Sarkissian, C. N., Wang, L., Kim, W., Straub, M., Patch, M. G., Chen, L., Striepeke, S., Fitzpatrick, P., Lemontt, J. F., O'Neill, C., Scriver, C. R., and Stevens, R. C. (2005) Development of pegylated forms of recombinant *Rhodosporidium toruloides* phenylalanine ammonia-lyase for the treatment of classical phenylketonuria, *Mol. Ther. 11*, 986−989.
33. Ikeda, K., Schiltz, E., Fujii, T., Takahashi, M., Mitsui, K., Kodera, Y., Matsushima, A., Inada, Y., Schulz, G. E., and Nishimura, H. (2005) Phenylalanine ammonia-lyase modified with polyethylene glycol: Potential therapeutic agent for phenylketonuria, *Amino Acids 29*, 283−287.
34. Appert, C., Logemann, E., Hahlbrock, K., Schmid, J., and Amrhein, N. (1994) Structural and catalytic properties of the four phenylalanine ammonia-lyase isoenzymes from parsley (*Petroselinum crispum* Nym.), *Eur. J. Biochem. 225*, 491−499.

BI061774G